



LAWRENCE
LIVERMORE
NATIONAL
LABORATORY

Measuring the hot-electron population using time-resolved, hard x-ray detectors on the NIF

M. Hohenberger, N. E. Palmer, G. LaCaille, E. L.
Dewald, L. Divol, E. J. Bond, T. Doeppner, J. J. Lee, J.
D. Salmonson, C. A. Thomas, D. K. Bradley, C. Stoeckl,
T. C. Sangster

August 8, 2013

SPIE Optics and Photonics 2013
San Diego, CA, United States
August 25, 2013 through August 29, 2013

Disclaimer

This document was prepared as an account of work sponsored by an agency of the United States government. Neither the United States government nor Lawrence Livermore National Security, LLC, nor any of their employees makes any warranty, expressed or implied, or assumes any legal liability or responsibility for the accuracy, completeness, or usefulness of any information, apparatus, product, or process disclosed, or represents that its use would not infringe privately owned rights. Reference herein to any specific commercial product, process, or service by trade name, trademark, manufacturer, or otherwise does not necessarily constitute or imply its endorsement, recommendation, or favoring by the United States government or Lawrence Livermore National Security, LLC. The views and opinions of authors expressed herein do not necessarily state or reflect those of the United States government or Lawrence Livermore National Security, LLC, and shall not be used for advertising or product endorsement purposes.

Measuring the hot-electron population using time-resolved, hard x-ray detectors on the NIF

M. Hohenberger¹, N. E. Palmer², G. LaCaille², E. L. Dewald², L. Divol², E. J. Bond², T. Döppner², J. J. Lee³, J. D. Salmonson², C. A. Thomas², D. K. Bradley², C. Stoeckl¹, and T. C. Sangster¹

¹Laboratory for Laser Energetics, University of Rochester, 250 East River Road, Rochester, NY 14623-1299, USA

²Lawrence Livermore National Laboratory, 7000 East Avenue, Livermore, CA 94551, USA

³National Security Technologies LLC, 161 S. Vasco Road, Suite A, Livermore, CA 94551, USA

ABSTRACT

In laser-driven inertial confinement fusion, hot electrons can preheat the fuel and prevent compression of the capsule to ignition conditions. Measuring the hot-electron population in these high-intensity, laser-driven experiments is key to understanding the laser–plasma interaction and the resulting target evolution. This can be inferred from the bremsstrahlung generated by the interaction of the hot electrons with the target. At the National Ignition Facility (NIF), the filter-fluorescer x-ray diagnostic (FFLEX), a multichannel, hard x-ray spectrometer operating in the 20- to 500-keV range, was recently upgraded to provide time-resolved measurements of the bremsstrahlung spectrum. Characterization data is presented for the upgraded setup, as well as recent results from ignition-scale experiments.

Keywords: National Ignition Facility (NIF), inertial confinement fusion (ICF), x-ray diagnostics, FFLEX

1. INTRODUCTION

In inertial confinement fusion (ICF), a capsule containing cryogenic deuterium–tritium (D–T) fusion fuel is rapidly compressed to high temperatures and areal densities sufficient for thermonuclear fusion.¹ If enough α particles are generated by D–T fusion reactions in the central hot spot of an imploded capsule deposit their energy in the compressed core, the capsule ignites. The energy released via the fusion burn can exceed the incident driver energy and the fusion gain exceeds unity when the confinement time determined by the fuel-mass inertia is sufficiently long. Demonstrating this concept is the main goal of ICF research.¹ In laser-driven ICF, the compression drive is provided by coupling laser energy into an ablator surrounding a spherical fuel capsule, either through symmetric, direct irradiation of the fusion target,² or indirectly via a thermal x-ray bath generated from laser illumination of the inner walls of a cavity (hohlraum).³ A key requirement for reaching the high fuel pressures required for ignition is keeping the DT fuel on a sufficiently low entropy, near Fermi degeneracy.¹

Current experiments on the National Ignition Facility (NIF)⁴ aim at maintaining low fuel entropy via shaped laser pulses for precise merging of multiple shock waves inside an ignition target. A key concern is energetic electrons generated through laser–plasma interactions (LPI’s) in the ablating hohlraum walls or the capsule ablator material. These can penetrate the ignition target and prematurely heat the fuel, raising the fuel adiabat and resulting in a lower compression and target performance. The acceptable level of hot-electron preheat increases as the capsule is being compressed,^{5,6} such that a precise understanding of the history of hot-electron generation in ignition experiments is vital for assessing its impact on the target performance.⁷

As the energetic electrons interact with the ablator or the hohlraum walls, they lose energy via collisions and in the form of bremsstrahlung emission. A simple formula relating an observed x-ray spectral-intensity distribution to a Maxwellian hot-electron population is given by the thick target bremsstrahlung equation,⁸

$$I \left[\frac{\text{keV}}{\text{keV} \cdot \text{sr}} \right] = \frac{5 \times 10^{11}}{4\pi} \cdot \frac{Z^*}{79} \cdot E_{\text{hot}} [J] \exp \left[-\frac{h\nu}{kT_{\text{hot}}} \right]. \quad (1)$$

$Z^* = \langle Z^2 \rangle / \langle Z \rangle$ is the average atomic number and E_{hot} is the energy content in the hot-electron population at temperature kT_{hot} . To quantify the hot-electron population in laser-driven experiments on the NIF, an absolutely calibrated filter-fluorescer x-ray diagnostic (FFLEX) measures the bremsstrahlung spectrum in the 20- to 500-keV range. FFLEX has been in operation on the NIF as a time-integrated diagnostic since 2004,⁹ but has recently been upgraded to provide temporal resolution. This paper describes the upgraded diagnostic and its characterization.

2. THE FFLEX DIAGNOSTIC

FFLEX consists of ten separate, time-resolved detectors, filtered to cover x-ray energies in the 20- to 500-keV range. FFLEX is positioned on the equator of the NIF target chamber at port (90,110). A schematic of Channels 2 and 9 is shown in Fig. 1, with the inset showing a photograph of the diagnostic mounted in the NIF Target Bay. Each channel comprises a fast BaF₂ scintillator, a UV filter, and a photomultiplier tube (PMT). BaF₂ has a decay time of ~700 ps and exhibits efficient absorption for x-ray energies as high as 500 keV. The UV filters have an ~40-nm bandpass centered at 220 nm and a peak transmittance of 30% to 40%. These filters isolate the 220-nm fast-decay component of BaF₂ from the 310-nm slow-decay component and reduce the light yield from the scintillator. The PMT's are Hamamatsu R5320 with a bialkali photocathode and a rise time of ~700 ps. A negative bias ranging from 700 V to 2500 V is applied to the photocathode. The gain scales approximately with the seventh power of the bias, giving a dynamic operating range over roughly four orders of magnitude. The anode of the PMT is run directly to the 50-Ω input of a 2.5-GHz Tektronix oscilloscope recording the signal at 10 GSamples/s, with two FFLEX channels sharing one oscilloscope. Timing is provided by an optical fiducial synchronized to the NIF laser clock at approximately 50 ns before the laser arrival, with a timing jitter of less than 20 ps. This is combined with the FFLEX signal via an optical-to-electrical converter and gives an absolute reference to time the x-ray signal relative to the laser pulse.

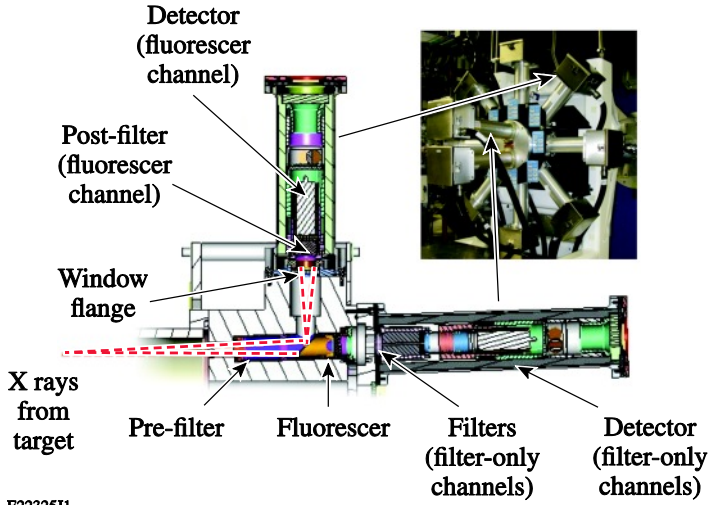


Figure 1. Schematic of FFLEX Channels 2 and 9. Inset: photograph of FFLEX mounted on the NIF target chamber.

E22325J1

Detectors 1–8 include a pre-filter, fluorescer, and post-filter, and are designed in pairs of narrow- and broadband detectors. The post-filters are the same material as the fluorescers and reduce the signal generated off the fluorescer foil. The fluorescer and pre-filter combination define the low-energy and high-energy cutoffs of the detector response. Detectors 9 and 10 employ filter-only setups and share the same line-of-sight with Channels 2 and 6, respectively. Table 1 summarizes the filter and fluorescer data of Channels 1–8; the combination of filters used for the filter-only channels are listed in Table 2. The transmission curves for the filter-fluorescer and filter-only setups are shown in Fig. 2.

Table 1. Filter-fluorescer setup for Channels 1–8.

Channel	Pre-filter	Fluorescer	Post-filter	Fluorescer edge (keV)	Pre-filter edge (keV)
1	Mo 91.0 μm	Y 24.2 μm	Y 18.9 μm	17.0	20.0
2	Sn 74.3 μm	Y 31.8 μm	Y 22.5 μm	17.0	29.3
3	Sn 353 μm	Ag 34.1 μm	Ag 6.8 μm	25.5	29.3
4	Mo 113 μm	Ag 29.6 μm	Ag 9.5 μm	25.5	20.0
5	Ta 526 μm	Yb 170 μm	Yb 42.2 μm	61.3	67.4
6	Pb 794 μm	Yb 160 μm	Yb 40.4 μm	61.3	88.0
7	Pb 801 μm	Au 105 μm	Au 25.5 μm	80.7	88.0
8	Ta 525 μm	Au 111 μm	Au 25.8 μm	80.7	67.4

Table 2. Filter setup for Channels 9 and 10.

Channel	Filter 1	Filter 2	Filter 3	Filter 4	Filter 5
9	Sn 74.3 μm	Y 31.8 μm	Cu 5 mm	Al 3 mm	—
10	Pb 794 μm	Yb 160 μm	Pt 0.8 mm	Cu 5 mm	Al 3 mm

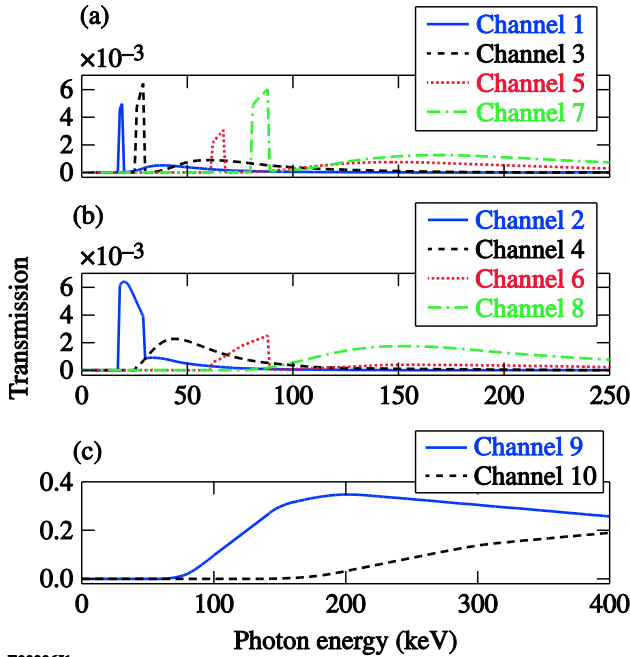


Figure 2. FFLEX channel filter-transmission curves. Channels are paired in narrowband/broadband (odd/even channel number) combinations for Channels 1–8. Channels 9 and 10 are high-energy channels measuring T_{hot} components above 100 keV.

E22326J1

Each detector is separately assembled in a PEEK housing that is seated inside an EMI tight enclosure that contains lead shielding to eliminate noise. An initial version of the FFLEX housing for the newly time-resolved detectors exhibited insufficient shielding. This resulted in significant background, particularly at late times and after the end of the laser drive. An example for such a data set is displayed in Fig. 3(a), with the solid blue line showing raw FFLEX data and the dashed line marking the laser pulse. The experiment was part of the Keyhole-Target Campaign to measure shock strength and relative shock timing inside the fuel of an imploding capsule.¹⁰ In this experiment (shot N130423) a NIF hohlraum was driven with ~ 1.1 -MJ and 350-TW peak power. The signal observed by FFLEX is expected to result from

energetic electrons interacting with the Au plasma inside the hohlraum. Since the lifetime of these electrons is less than 100 ps, once the laser has turned off the FFLEX trace is expected to drop quickly on the time scale of the detector's decay time (~ 3 ns, see Fig. 6). Instead Fig. 3(a) shows a significant FFLEX signal after the end of the laser pulse, extending over tens of nanoseconds. These observations led to an upgrade of the FFLEX housing with a modified window flange (see Fig. 1) and an additional Pb bracelet that wraps each detector (not shown in Fig. 1), adding 1 in. of lead shielding around each scintillator and PMT. Figure 3(b) shows raw FFLEX data of a recent keyhole-target shot (shot N130517) with very similar experimental conditions to the data from Fig. 3(a), but with the additional shielding deployed. As expected, the data in Fig. 3(b) does not exhibit the signal following the end of the laser pulse (dashed line)..

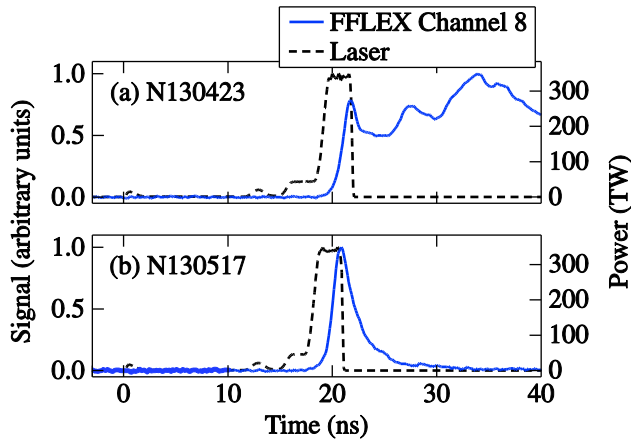


Figure 3. FFLEX signal traces (a) before and (b) after upgrading the FFLEX shielding. The dashed line shows the laser-power profile and the solid line is the raw FFLEX waveform. As a result of the upgraded shielding, the late-time background in the FFLEX data after the end of the laser pulse has been removed.

E22327J1

3. CHARACTERIZATION

Calibrations were performed to quantify each detector's x-ray sensitivity, PMT space-charge saturation, impulse response function (IRF), and the detector transit time.

The absolute sensitivity of each FFLEX detector is determined by measuring the PMT's dc current while exposed to an x-ray source of known intensity and spectral composition. The high-energy x-ray source (HEX) at NSTec Livermore Operations served as a calibration source.¹¹ HEX uses a high-energy x-ray tube to excite K-shell fluorescence in a fluorescer foil and is capable of delivering near monoenergetic x-ray energies in the range of 8 keV (Cu K_{α}) to 111 keV (U K_{β}). The x-ray emission is collimated and its total flux is measured with an absolutely calibrated, energy-dispersive high-purity germanium detector (HPGe). Placing an FFLEX channel in the same position as the HPGe reference exposes it to the same flux, thereby relating the FFLEX PMT current to the incident x-ray flux at a known K-shell energy. Taking the dark current into account for background subtraction, and multiplying with the 50- Ω input impedance of the oscilloscope, yields the channel sensitivity in units of V ns/keV. This relates the total area under the oscilloscope waveform from an FFLEX detector to the x-ray energy incident on the scintillator.

To quantify the uncertainty of this measurement, the absolute sensitivity of a single FFLEX detector biased at -1700 V was measured in multiple configurations. This included measurements at different x-ray energies from 22 keV (Ag K_{β}) to 111 keV (U K_{β}), with x-ray beams of different sizes and at two separate distances to the HEX source. Within the error of the measurement, the detector showed a flat response over the measured energy range, and the 14 individual setups yielded a standard deviation in the calculated sensitivity of 17%. The remaining FFLEX detectors were calibrated over the full operating bias range of -700 V to -2500 V in 200-V steps, with the x-ray source energies selected to match the operating range of the specific detector. Despite the calibration being limited to below ~ 110 keV, the BaF₂ light yield per incident energy depends only weakly on the photon energy above 100 keV and the detector sensitivity can be expected to be flat beyond the calibrated energies.¹²

For signals of high enough magnitude, dynode-based PMT's are expected to saturate because of space-charge current limitations, as opposed to charge depletion. The PMT current reaches an upper limit and the output of the PMT broadens

temporally, while the integrated charge will remain proportional to the total incident light. To avoid temporal broadening of the measured FFLEX signal, it is important to operate the detector below this space-charge saturation limit. The voltage on the oscilloscope at which signal broadening occurs was measured by focusing a 5-ns, 400-nm laser onto the photocathode of the PMT. By varying the incident energy, the signal was increased until the detector response started to broaden. Figure 4 shows the average space-charge saturation limit as a function of the applied bias voltage, with the error bars denoting the highest and lowest values measured. To avoid nonlinearity effects prior to reaching the saturation limit, the detectors are typically operated at signal levels of 10% to 25% of saturation.

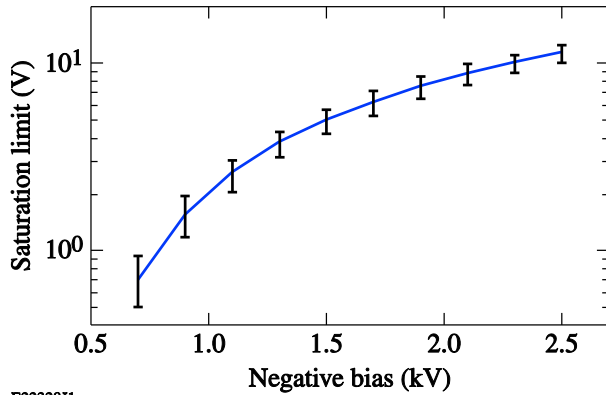


Figure 4. FFLEX space-charge limit of the signal voltage as a function of the applied bias. The solid line is the average of all ten detectors and the error bars denote minimum and maximum measured values.

E22328J1

The transit time of the electrons from the PMT photocathode to the anode is a function of the applied bias voltage. This was measured by focusing an 80-ps, 400-nm laser pulse directly onto the PMT photocathode and comparing the laser arrival time, as measured by a photodiode, with the time of the measured PMT peak current. Figure 5 shows the difference in the delay between the peak signal on the photodiode and the PMT as a function of bias voltage. This is well fit by

$$t[\text{ns}] = 10 \sqrt{\frac{2250}{V_{\text{bias}}[\text{V}]}} \quad (2)$$

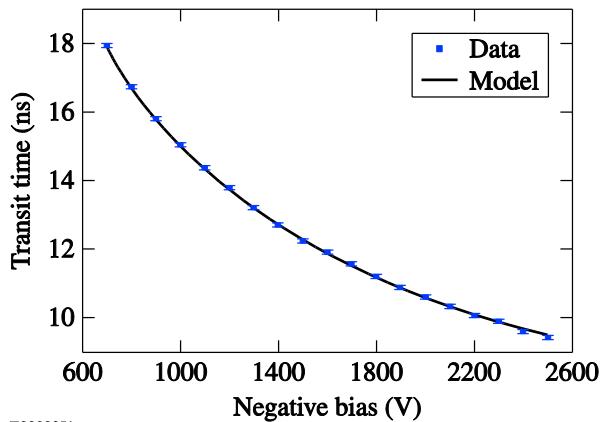


Figure 5. PMT transit time as a function of the applied bias voltage.

E22329J1

A dedicated NIF timing shot is used to establish synchronization of all ten FFLEX channels. A typical NIF timing shot tuned for hard x-ray emission uses all 192 NIF beams delivering a pulse shape with a total energy of ~14 kJ and consisting of a 1-ns foot at ~0.5 TW followed by an ~90-ps laser impulse reaching ~80 TW. The laser is focused onto a 6- μm Au foil coated with 5 μm of CH. The laser prepulse ablates the CH coating, thereby setting up a plasma

atmosphere that enhances coupling of the incident high-intensity impulse, which then generates hot electrons resulting in hard x-ray emission concurrent with the laser impulse. The errors in determining the timing of peak emission, laser timing, and fiducial jitter, as well as that introduced by the PMT transit time, yields an uncertainty in the FFLEX oscilloscope traces of ~ 170 ps. With a systematic uncertainty in the impulse response function (see below) of ~ 150 ps, the timing error after deconvolution increases to 230 ps.

Any x-ray signal recorded by FFLEX will be convolved with the system's impulse response function (IRF) and to extract the temporal profile of the incident signal from the data, the detector's IRF must be accurately known. The x-ray IRF of two FFLEX detectors was measured offline with the Comet laser at the Jupiter Laser Facility (JLF)¹³ before installation on the NIF. A 5-J, 1053-nm, subpicosecond laser was focused onto a Cu target to generate an x-ray signal that was then recorded with individual FFLEX detectors nominally set up using the same configuration as on the NIF (cabling, oscilloscope, etc.). The FFLEX signal is recorded in 100-ps steps such that the x-ray emission from the Cu can be regarded as a delta function and the measured FFLEX signal is a direct representation of the system's response. Multiple measurements of the bias-dependent IRF's were obtained for a set of bias voltages on both detectors, and, as expected, no significant variation of the system response was observed between the two FFLEX channels.

The NIF timing shots act as an *in-situ* measurement of the detector's impulse response. Because of low signal, this is limited to high-gain settings with biases typically exceeding -2200 V. At these voltages, the *in-situ* rise and decay times of the detector's signals proved faster than the offline measurements, indicating that the experimental setup for offline measurements did not fully reproduce the setup used on the NIF. The offline IRF's were scaled to match the *in-situ* response and the same correction factor was applied to the IRF's used for lower bias settings. Figure 6 shows examples of the FFLEX IRF at various bias voltages. As expected, the impulse response becomes faster with increased bias since the PMT transit time is shortened and the current waveform dispersion during transit from photocathode to anode is reduced.

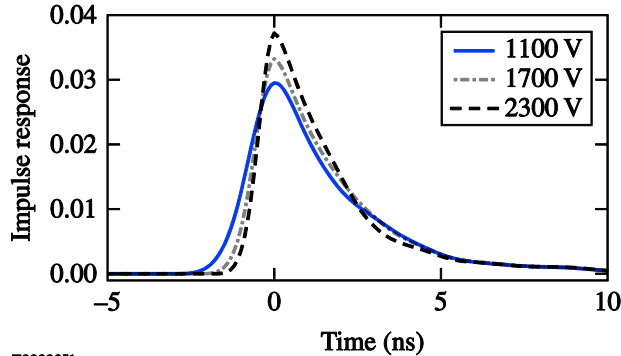


Figure 6. FFLEX impulse response function at an operating bias of -1.1 kV (solid line), -1.7 kV (dashed-dotted line), and -2.3 kV (dashed line).

E22330J1

4. DATA ANALYSIS

To estimate the hot-electron temperatures generating the measured FFLEX signals, an exponentially falling hard x-ray spectrum following Eq. (1) is assumed. The expected, time-integrated signal of the i th FFLEX channel resulting from a hot-electron population with n temperature components can be written as

$$I_i [\text{V ns}] = \frac{5 \times 10^{11}}{4\pi} \cdot \frac{Z^*}{79} \cdot S_i \int_0^\infty \left\{ F(\nu) T_i(\nu) \sum_n E_{\text{hot},n} \exp[-h\nu/kT_{\text{hot},n}] d\nu \right\}. \quad (3)$$

Here S_i is the channel and bias-dependent detector sensitivity multiplied with the detector solid angle, $F(\nu)$ is the energy-dependent transmission function of any material between the x-ray source and the detector (e.g., the hohlraum), and $T_i(\nu)$ denotes the spectral sensitivity of the i th FFLEX channel as determined by the filter-fluorescer combination (see

Tables 1 and 2). Based on the experimental conditions and the temporal history of the x-ray signal, a two- to five-parameter model of the x-ray spectrum is fit to the data. A typical indirect-drive-ignition experiment exhibits a two-temperature distribution of the hot-electron population inside the hohlraum,¹⁴ with the low-temperature component ($T_1 \sim 20$ keV) being attributed to stimulated Raman scattering,¹⁵ and a hotter component of ($T_2 \sim 100$ keV) likely caused by interaction close to quarter-critical density (e.g., two-plasmon decay).¹⁶ For a given set of FFLEX data, the hot-electron temperature is determined through an iterative fitting process and a χ^2 analysis. In hohlraum experiments, it was found that additionally including K_α and K_β emission as a fitting parameter (rather than solving it self-consistently) significantly improves the fit. A result of such a time-integrated analysis is shown Fig. 7 for the same experiment as discussed in Fig. 3(b). Here, the solid line is the extracted emission spectrum inside the hohlraum as a function of x-ray energy, with the data points denoting the experimental FFLEX data for each channel. With temperatures of $T_1 = 20 \pm 5$ keV and $T_2 = 86 \pm 11$ keV, the energy contents in each temperature component were calculated to be $E_1 = 11 \pm 2.3$ kJ and $E_2 = 393 \pm 130$ J.

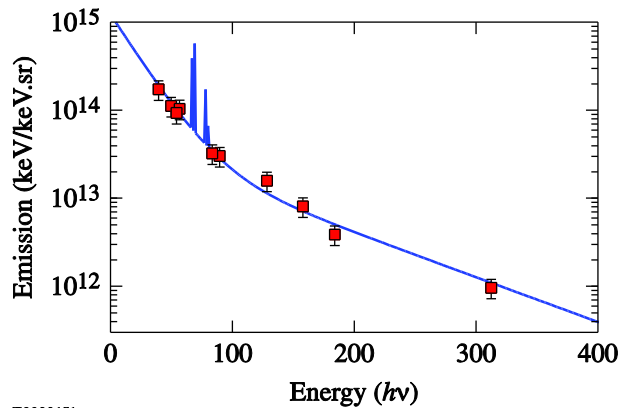


Figure 7. Result of the time-integrated FFLEX analysis for shot N130517. The data points are the total emission as measured by the individual FFLEX channels and the solid line is a two-temperature fit to the experimental data with $E_1 = 11 \pm 2.3$ kJ, $T_1 = 20 \pm 5$ keV, $E_2 = 393 \pm 130$ J, and $T_2 = 86 \pm 11$ keV.

E22331J1

To take advantage of the time-resolved capabilities of the upgraded FFLEX diagnostic, the oscilloscope waveforms must first be deconvolved to remove the detector-imposed IRF's and produce a signal representative of the time-varying x-ray flux incident onto the FFLEX detector. To do this, the iterative deconvolution method of Nagy and Strakoš¹⁷ is used, a modification of the steepest descent algorithm to minimize least-squares differences between the measured signal and the convolution of the deconvolved signal with the IRF.

An example for a time-resolved analysis is shown in Fig. 8, using the same data as discussed in Fig. 7, but analyzed in 300-ps intervals. For simplicity, T_1 was fixed at 20 keV, as for the time-integrated analysis. The solid line in Fig. 8(a) shows the hot-temperature component T_2 as a function of time, while the dashed line denotes the laser power. Note that the time axis is 18 ns to 21.5 ns, corresponding to the peak drive of the laser [compare Fig. 3(b)]. FFLEX recorded no signal prior to this time, and the high-energy Channels 9 and 10 did not measure any significant signal until after 19.5 ns. Accordingly, the data for T_2 starts only at that time, followed by a continuous rise until the end of the laser pulse, and peaking at ~ 100 keV. Figure 8(b) shows the energy content for both temperature components on the same time scale and in units of J/ns. The blue solid line is the energy content E_1 , and the red dashed line denotes the hot-energy component E_2 . Similar to the time-integrated result, E_1 exceeds E_2 by approximately one order of magnitude. E_1 peaks much earlier than E_2 at ~ 19 ns, while the hot component follows the temporal evolution of T_2 and increases until the laser power drops at ~ 21 ns.

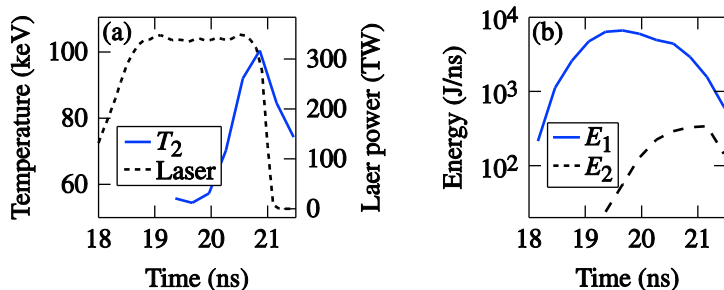


Figure 8. Result of the time-resolved FFLEX analysis for shot N130517 in steps of 300 ps. (a) The hot-component temperature T_2 peaks at ~ 100 keV at the end of the laser drive (dashed line). (b) The energy component E_2 follows the temporal evolution of T_2 and peaks at the end of the drive, while E_1 peaks earlier at around 19 ns.

E22332J1

In conclusion, FFLEX is a hard x-ray detector in operation at the National Ignition Facility and is used to infer the hot-electron population in ignition experiments. The diagnostic consists of ten separate channels filtered to be sensitive to x rays in the 20- to 500-keV range. FFLEX has been in operation as a time-integrated diagnostic since 2004, but has recently been upgraded to provide absolutely calibrated, fully time-resolved measurements. Recent results of the hot-electron temperature population in an ignition-scale, indirect-drive experiment show a two-temperature distribution with the hot component being delayed in time with respect to the colder component, and peaking toward the end of the drive.

ACKNOWLEDGMENT

This material is based upon work supported by the Department of Energy National Nuclear Security Administration under Award Number DE-NA0001944, the University of Rochester, and the New York State Energy Research and Development Authority. Lawrence Livermore National Laboratory is operated by Lawrence Livermore National Security, LLC, for the U.S. Department of Energy, National Nuclear Security Administration under Contract DE-AC52-07NA27344. The support of DOE does not constitute an endorsement by DOE of the views expressed in this article.

REFERENCES

- [1] Atzeni, S. and Meyer-ter-Vehn, J., [The Physics of Inertial Fusion: Beam Plasma Interaction, Hydrodynamics, Hot Dense Matter], International Series of Monographs on Physics, Clarendon Press, Oxford (2004).
- [2] S. Skupsky, J. A. Marozas, R. S. Craxton, R. Betti, T. J. B. Collins, J. A. Delettrez, V. N. Goncharov, P. W. McKenty, P. B. Radha, T. R. Boehly, J. P. Knauer, F. J. Marshall, D. R. Harding, J. D. Kilkenny, D. D. Meyerhofer, T. C. Sangster, and R. L. McCrory, "Polar direct drive on the National Ignition Facility," Phys. Plasmas 11, 2763 (2004).
- [3] Lindl, J. D., Amendt, P., Berger, R. L., Glendinning, S. G., Glenzer, S. H., Haan, S. W., Kauffman, R. L., Landen, O. L., Suter, L. J., "The physics basis for ignition using indirect-drive targets on the National Ignition Facility," Phys. Plasmas 11, 339 (2004).
- [4] Moses, E. I., "The National Ignition Facility: Status and plans for the experimental program," Fusion Sci. Technol. 44(1), 11–18 (2003).
- [5] Dewald, E. L., Suter, L. J., Thomas, C., Hunter, S., Meeker, D., Meezan, N., Glenzer, S. H., Bond, E., Kline, J., Dixit, S., Kauffman, R. L., Kilkenny, J. and Landen, O. L., "First hot electron measurements in near-ignition scale hohlraums on the National Ignition Facility," J. Phys., Conf. Ser. 244(2), 022074 (2010).
- [6] Dewald, E. L., Thomas, C., Hunter, S., Divol, L., Meezan, N., Glenzer, S. H., Suter, L. J., Bond, E., Kline, J. L., Celeste, J., Bradley, D., Bell, P., Kauffman, R. L., Kilkenny, J. and Landen, O. L., "Hot electron measurements in ignition relevant hohlraums on the National Ignition Facility," Rev. Sci. Instrum. 81(10), 10D938 (2010).
- [7] Stoeckl, C., Glebov, V. Yu., Meyerhofer, D. D., Seka, W., Yaakobi, B., Town, R. P. J., and Zuegel, J. D., "Hard x-ray detectors for OMEGA and NIF," Rev. Sci. Instrum. 72, 1197 (2001).
- [8] Drake, R. P., Turner, R. E., Lasinski, B. F., Williams, E. A., Estabrook, K., Kruer, W. L., Campbell, E. M. and Johnston, T. W., "X-ray emission caused by Raman scattering in long-scale-length plasmas," Phys. Rev. A 40(6), 3219–3225 (1989).

- [9] McDonald, J. W., Kauffman, R. L., Celeste, J. R., Rhodes, M. A., Lee, F. D., Suter, L. J., Lee, A. P., Foster, J. M. and Slark, G., “Filter-fluorescer diagnostic system for the National Ignition Facility,” *Rev. Sci. Instrum.* 75(10), 3753–3755 (2004).
- [10] Robey, H. F., Boehly, T. R., Celliers, P. M., Eggert, J. H., Hicks, D., Smith, R. F., Collins, R., Bowers, M. W., Krauter, K. G., Datte, P. S., Munro, D. H., Milovich, J. L., Jones, O. S., Michel, P. A., Thomas, C. A., Olson, R. E., Pollaine, S., Town, R. P. J., Haan, S., Callahan, D., Clark, D., Edwards, J., Kline, J. L., Dixit, S., Schneider, M. B., Dewald, E. L., Widmann, K., Moody, J. D., Döppner, T., Radousky, H. B., Throop, A., Kalantar, D., DiNicola, P., Nikroo, A., Kroll, J. J., Hamza, A. V., Horner, J. B., Bhandarkar, S. D., Dzenitis, E., Alger, E., Giraldez, E., Castro, C., Moreno, K., Haynam, C., LaFortune, K. N., Widmayer, C., Shaw, M., Jancaitis, K., Parham, T., Holungal, D. M., Walters, C. F., Haid, B., Mapoles, E. R., Sater, J., Gibson, C. R., Malsbury, T., Fair, J., Trummer, D., Coffee, K. R., Burr, B., Berzins, L. V., Choate, C., Brereton, S. J., Azevedo, S., Chandrasekaran, H., Eder, D. C., Masters, N. D., Fisher, A. C., Sterne, P. A., Young, B. K., Landen, O. L., Wonterghem, B. M. V., MacGowan, B. J., Atherton, J., Lindl, J. D., Meyerhofer, D. D. and Moses, E., “Shock timing experiments on the National Ignition Facility: Initial results and comparison with simulation,” *Phys. Plasmas* 19(4), 042706 (2012).
- [11] Lee, J. J., Haugh, M. J., LaCaille, G. and Torres, P., “Calibrating of x-ray detectors in the 8 to 111 keV energy range and their application to diagnostics on the National Ignition Facility,” *Proc. SPIE* 8505, 850508 (2012).
- [12] Mengesha, W., Taulbee, T. D., Valentine, J. D. and Rooney, B. D., “ $\text{Gd}_2\text{SiO}_5(\text{Ce}^{3+})$ and BaF_2 measured electron and photon responses,” *Nucl. Instrum. Methods Phys. Res. A* 486(1–2), 448–452 (2002).
- [13] Nagel, S. R., Hilsabeck, T. J., Bell, P. M., Bradley, D. K., Ayers, M. J., Barrios, M. A., Felker, B., Smith, R. F., Collins, G. W., Jones, O. S., Kilkenny, J. D., Chung, T., Piston, K., Raman, K. S., Sammulu, B., Hares, J. D. and Dymoke-Bradshaw, A. K. L., “Dilation x-ray imager a new/faster gated x-ray imager for the NIF,” *Rev. Sci. Instrum.* 83(10), 10E116 (2012).
- [14] Döppner, T., Thomas, C. A., Divol, L., Dewald, E. L., Celliers, P. M., Bradley, D. K., Callahan, D. A., Dixit, S. N., Harte, J. A., Glenn, S. M., Haan, S. W., Izumi, N., Kyrala, G. A., LaCaille, G., Kline, J. K., Kruer, W. L., Ma, T., MacKinnon, A. J., McNaney, J. M., Meezan, N. B., Robey, H. F., Salmonson, J. D., Suter, L. J., Zimmerman, G. B., Edwards, M. J., MacGowan, B. J., Kilkenny, J. D., Lindl, J. D., Van Wonterghem, B. M., Atherton, L. J., Moses, E. I., Glenzer, S. H. and Landen, O. L., “Direct measurement of energetic electrons coupling to an imploding low-adiabat inertial confinement fusion capsule,” *Phys. Rev. Lett.* 108(13), 135006 (2012).
- [15] Offenberger, A. A., Fedosejevs, R., Tighe, W. and Rozmus, W., “Stimulated Raman backscatter from a magnetically confined plasma column,” *Phys. Rev. Lett.* 49(6), 371–375 (1982).
- [16] Regan, S. P., Meezan, N. B., Suter, L. J., Strozzi, D. J., Kruer, W. L., Meeker, D., Glenzer, S. H., Seka, W., Stoeckl, C., Glebov, V. Y., Sangster, T. C., Meyerhofer, D. D., McCrory, R. L., Williams, E. A., Jones, O. S., Callahan, D. A., Rosen, M. D., Landen, O. L., Sorce, C. and MacGowan, B. J., “Suprathermal electrons generated by the two-plasmon-decay instability in gas-filled *hohlraums*,” *Phys. Plasmas* 17(2), 020703 (2010).
- [17] Nagy, J. and Strakoš, Z., “Enforcing nonnegativity in image reconstruction algorithms,” *Proc. SPIE* 4121, 182–190 (2000).